Desalination and Water Treatment
www.deswater.com
doi: 10.5004/dwt.2020.25239

183 (2020) 335–345
April

Efficient photo-Fenton degradation of dye and drug molecules over Fe_2O_3/C composite with 1,4-benzoquinone as sacrificial agent

Jing Zhou

Department of Energy and Material Engineering, Shandong Polytechnic College, Jining 272400, China, email: zjjscd@126.com

Received 23 June 2019; Accepted 26 November 2019

ABSTRACT

In order to efficiently deal with environmental pollution caused by industrial wastewater and drug molecules, a novel Fenton catalytic system of Fe_2O_3/C-(1,4-benzoquinone) has been successfully developed, which shows obviously enhanced Fenton catalytic activities for organic pollutants (Rhodamine B and ibuprofen) degradation than Fe_2O_3/C composite. The Fenton catalytic activity of the Fe_2O_3/C composite with 1,4-benzoquinone (BQ) as cocatalyst is 10.14 times higher than that of Fe_2O_3/C composite. Furthermore, with BQ as cocatalyst, the catalytic activity of the Fe_2O_3/C composite is 35.5 times and 15.8 times that of Fe_2O_3 and carbon, respectively. The concentration ratios of carbon in the Fe_2O_3/C composite and BQ in the system are also discussed, demonstrating that the 50 wt% carbon in Fe_2O_3/C composite and 3 wt% BQ in the system are the optimized conditions. The carbon in the Fe_2O_3/C composite acts as an adsorbent of organic pollutants and BQ. The contribution of BQ in the Fenton system is reflected in the scavenging of $^{\bullet}O_2^-$ radical and photogenerated electrons, which promotes the production of Fe^{II} and photogenerated hole, resulting in a rapid degradation process. Furthermore, the BQ is also degraded with the degradation of organic pollutants, which does not cause secondary pollution to the water. This study sheds new light on the design and fabrication of novel Fenton catalytic system to solve the environmental crisis.

Keywords: Fe_2O_3/C composite; Photo-Fenton degradation; 1,4-Benzoquinone; Environmental pollution

1. Introduction

Recently, great efforts have been made to deal with environmental pollution caused by industrial wastewater and drug molecules, which inevitably caused and still contributing great harm to human survival. Among various techniques, advanced oxidation technologies have been proved to be an effective solution owing to the advantage of strong oxidation, high efficiency, environment friendly, etc. [1–5]. The homogeneous Fenton reaction (Fe^{II}-H_2O_2) has high catalytic activity by producing reactive hydroxyl radical (·OH), which however, is limited by the precipitate of ferric hydroxide [6–8]. To address the problem of iron sludge, heterogeneous Fenton reaction (Fe^{III}-H_2O_2) has attracted much attention. Since the kinetics of reaction of Fe^{III} with H_2O_2 to produce Fe^{II} is sluggish, rigorous conditions (such as acid solution, high temperature or electrical energy) are usually necessary [9–11]. Hence, the development of efficient heterogeneous Fenton catalysis system is still a tremendous challenge.

To date, iron oxides have been extensively studied as heterogeneous Fenton catalysts, primarily because of their cost-effective, environmentally benign and low iron release [12–15]. However, the high surface energy of Fe_2O_3 nanoparticles leads to agglomeration, resulting in the decreased number of catalytic active sites. Moreover, the photo-Fenton

* Corresponding author.

catalytic activity of Fe_2O_3 is also hampered by the high electron–hole recombination rate and the low surface adsorption of organic pollutants [16]. At present, the main solution is to hybridize Fe_2O_3 with supports, such as TiO_2, SiO_2, C_3N_4, porous carbon, diamond, graphene oxide, etc. [17–22]. Besides, since the active species (•OH radical) play the most important role in catalytic degradation, another possible solution is to accelerate the reaction of Fe^{III} with H_2O_2 to produce Fe^{II} by increasing the consumption of $^{\bullet}O_2H$ radicals, which will facilitate the production of •OH radical.

According to the literatures, benzoquinone (BQ) can react with $^{\bullet}O_2H$ generated by the Fenton reaction very quickly, leading to the accelerated catalytic cycling of Fe^{3+}/Fe^{2+} in the solution containing iron ions and H_2O_2 [23,24]. Therefore, the benzoquinone may also play the same role in the suspension containing solid catalyst and H_2O_2. Inspired by this, we offer a viable solution to prepare Fe_2O_3/carbon (C) composite as heterogeneous Fenton catalyst and BQ as cocatalyst. With BQ as a cocatalyst, the Fe_2O_3/C composite demonstrates obviously increased photo-Fenton catalytic activity of degradation of organic pollutants (Rhodamine B and ibuprofen). The degradation constant (k) of the Fe_2O_3/C composite with BQ addition is 10.14 times as many as that of Fe_2O_3/C composite without BQ addition. The existence of BQ as a cocatalyst greatly increased the consumption of $^{\bullet}O_2H$ radicals and accelerated the reaction of Fe^{III} and H_2O_2 to produce Fe^{II}. Meanwhile, the carbon in the composite effectively increased the adsorption of organic pollutant. Furthermore, the Fe_2O_3/C composite with BQ also shown excellent structure stability. The enhanced Fenton catalytic performance is mainly contributed from the synergistic interaction of Fe_2O_3/C and BQ in the system. Moreover, the BQ is also degraded in the photo-Fenton process, which cannot cause secondary pollution.

2. Experiments

2.1. Synthesis of Fe_2O_3/C composite

All the chemicals were of analytical grade (Sinopharm Chemical Reagent Co., Ltd.) and used without any further purification. As a typical synthetic course (Fig. 1), 0.1 g of $FeCl_3$ and 0.05 g of $C_6H_{12}O_6$ were added in distilled water (3 mL) to form solution by ultrasound. After drying at 30°C, the dried product was first calcined at 220°C for 1 h (heating rate, 15°C/min), and then at 360°C for 2.0 h (heating rate of 5°C/min) under N_2 atmosphere. The obtained product was washed with water for three times, and then dried at 90°C in a vacuum oven for 12 h. The preparation of Fe_2O_3 and carbon was similar to the above method.

2.2. Characterization of catalytic activity

In a typical experiment, 0.05 g of Fe_2O_3/C and 1.5 mg BQ was added into a 100 mL solution (5 mg/L, RhB solution or ibuprofen solution), and then was stirred for 60 min. After adding 0.5 mL of H_2O_2 aqueous solution (30 wt%), 5 mL of the reaction mixture was taken out at a time interval of 5 min. The mixture was centrifuged before measuring the UV-vis absorption spectra. Fluorescence technique was carried out to measure the decomposition of H_2O_2 by using terephthalic acid as trapping agent [25,26].

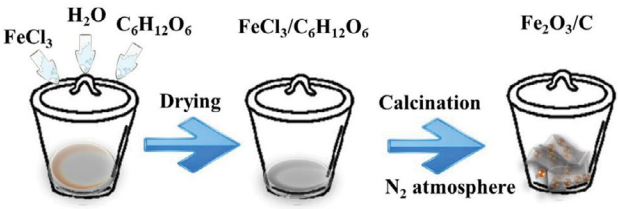

Fig. 1. Schematic illustration of the synthesis of Fe_2O_3/C composite.

The dominant reactions related to the photo-Fenton catalytic mechanism was represented by the expression:

$$Fe_2O_3/C \text{ are: } Fe^{3+} + H_2O_2 \rightarrow {}^{\bullet}O_2H + Fe^{2+} + H^+ \quad (1)$$

$$C_6H_4O_2 + {}^{\bullet}O_2^- \rightarrow O_2 + C_6H_4O_2^{\bullet -} \quad (2)$$

$$Fe^{2+} + H_2O_2 \rightarrow Fe^{3+} + {}^{\bullet}OH + OH^- \quad (3)$$

$$^{\bullet}OH + RhB \rightarrow \text{product} \quad (4)$$

$$^{\bullet}OH + C_6H_4O_2 \rightarrow \text{product} \quad (5)$$

2.3. Characterization

X-ray diffraction (XRD) technique on a D8 Advance diffractometer was carried out to identify the phase structure of the sample at room temperature. The morphology was characterized by TEM (JEM-2100) and SEM (S-4800). The energy dispersive X-ray spectrometry (EDS) at 15 kV was used to perform qualitative chemical analyses. The Fourier transform infrared (FTIR) spectra were measured on a Nicolet IS 10 spectrometer in the range of 400~4,000 cm^{-1} by KBr pellet method. The Brunauer–Emmett–Teller (BET) surface area was measured by N_2 adsorption technique at 77 K using a Pore Master-60 analyser. UV-vis spectrophotometer (Lambda-35, PerkinElmer) was used to measure the UV-vis absorption spectra. Fluorescence was analysed on a fluorescence spectrophotometer (F-4600). PerkinElmer PHI-5300 ESCA was used to measure X-ray photoelectron spectroscopy (XPS). Photoluminescence (PL) spectra was collected by HITACHI (F-2700). Mott–Schottky plots and electrochemical impedance spectroscopy (EIS) were obtained by the electrochemical analyser (CHI760E) with a standard three-electrode configuration in 0.01 M Na_2SO_4 solution. The Pt wire, saturated calomel electrode and fluorine-doped tin oxide (FTO) were used as counter electrode, reference electrode and working electrode, respectively. Photoelectro chemistry experiment was performed in a standard three-electrode cell system, which used Pt wire and Ag/AgCl as counter electrode and reference electrode, respectively.

3. Results and discussion

3.1. Characterization of Fe_2O_3/C composite

The structures of the samples were analyzed by XRD (Fig. 2a), which demonstrate that the obvious diffraction peaks of Fe_2O_3 match with the hematite phase (JCPDS no.

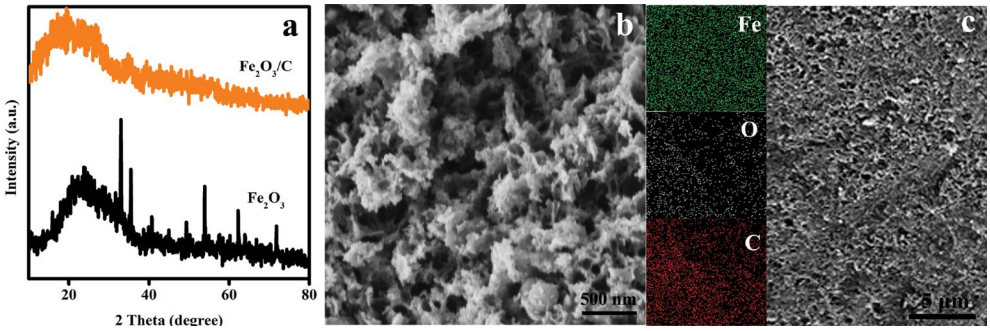

Fig. 2. (a) XRD patterns of Fe_2O_3 and Fe_2O_3/C composite, (b) SEM image of Fe_2O_3/C composite and (c) SEM image and the corresponding EDS elemental mapping images of Fe_2O_3/C composite.

89-0597). However, the XRD pattern of Fe_2O_3/C composite is amorphous, indicating the successful composite of Fe_2O_3 and carbon [27,28]. The morphology of Fe_2O_3/C composite studied by SEM measurement (Fig. 2b) shows that the Fe_2O_3/C composite consists of nanoparticles with porous structure and the Fe_2O_3 nanoparticles uniformly disperse in the carbon skeleton, suggesting the large contact area between Fe_2O_3 and C. In addition, the corresponding EDS spectrum of the Fe_2O_3/C composite was measured, which shows that all the Fe, O and C elements were detected. To ensure the homogeneity of each element, the corresponding EDS elemental mapping images of Fe, O and C (Fig. 2c) indicate that each element in Fe_2O_3/C composite is uniformly distributed in the particles. Compared with the morphology of the Fe_2O_3 composite, the surface of Fe_2O_3 is smooth and the particle size of Fe_2O_3 is several microns (Figs. S1a and b), suggesting the great contribution of carbon to decrease the size and increase the dispersity of Fe_2O_3. Therefore, the intimate contact between Fe_2O_3 and C in the composite presumably facilitates the charge-carrier transport and the adsorption for organic pollutant, resulting in the promotion of catalytic activity of Fe_2O_3.

Fourier transform infrared spectroscopy (FTIR) was measured to characterize the detail structure of the Fe_2O_3/C composite (Fig. 3a). Compared with the FTIR spectra of Fe_2O_3 in Fig. S2, the FTIR spectra of the Fe_2O_3/C exhibits the carbon-rich property in the composite. The spectrum of Fe_2O_3/C composite displays a band of strong intensity between 3,200 and 3,500 cm^{-1}, which are the signals of O–H. The peaks at 1,100 and 1,400 cm^{-1} are assigned to C–C and C–O groups, respectively. The peak at 1,650 cm^{-1} is due to the stretching vibration of the –C=O group. Therefore, the carbon contains many C–O groups, which could be propitious to adsorb organic pollutants [29–33]. Since the O and C elements observed are dispersed uniformly in the Fe_2O_3/C composite (Fig. 2b), the C–O groups are also packed on the product uniformly. For the sake of studying the optical absorption and band gap, the ultraviolet-visible diffusive reflectance spectra were measured (Fig. 3b), which shows that the Fe_2O_3/C composite has excellent light absorption. And the direct optical band gap (E_g) of the Fe_2O_3/C composite is 2.81 eV according to the transformed diffuse reflectance spectra (Fig. 3c). As for Fe_2O_3, the direct optical band gap (E_g) is 2.15 eV (Fig. S3), which is smaller than that of the Fe_2O_3/C composite. In addition, the Mott–Schottky plots of the Fe_2O_3/C composite and the Fe_2O_3 in Fig. 3d reveal that the conduction band (CB) of the Fe_2O_3/C decreased. The Fe_2O_3/C composite and Fe_2O_3 have the flat potentials of –0.40 V and –0.28 V vs. saturated calomel electrode (SCE), respectively, indicating that the CB potentials of Fe_2O_3/C composite and Fe_2O_3 are 0.25 and 0.37 V [34–37]. Accordingly, the corresponding potentials of valence band (VB) of Fe_2O_3/C composite and Fe_2O_3 are 3.06 and 2.52 V, respectively. Therefore, the composite structure of Fe_2O_3/C has obviously changed the band structure of Fe_2O_3.

The Fe_2O_3/C composite was further investigated by XPS analysis (Fig. 4). The result in Fig. S4 of full-range XPS spectrum of Fe_2O_3/C composite clearly demonstrates the photoelectron peaks of Fe, O and C elements, further verifying the coexistence of Fe_2O_3 and carbon in the composite. Furthermore, the element content of Fe, O and C in the composite shows that the molar ratio of Fe:O:C is 1:1.9:7.1. The mole ratio of Fe and O (1:1.9) in the composite is bigger than that in Fe_2O_3 (1:1.5). It indicates that there is excess oxygen in the carbon structure (C–O functional groups), which is consistent with the results in the FTIR spectrum (Fig. 3a). The binding energy peaks centered at 711.8 and 724.6 eV correspond to $Fe2p_{3/2}$ and $Fe2p_{1/2}$, respectively (Fig. 4a), suggesting the Fe^{III} state in the composite. The appeared satellite peak of $Fe2p_{3/2}$ in Fig. 4a is the characteristic satellite peak of Fe_2O_3, indicating that the iron oxide in the composite is Fe_2O_3 [38–41]. The XPS spectrum of O1s in Fig. 4b shows two peaks of binding energy at 531.7 and 533.2 eV, which are assigned to Fe–O and water species [42]. The peaks of binding energy centered at 284.6 and 285.8 eV correspond to C–C and C–O, respectively (Fig. 4c). According to the XPS results (Fig. 4d), the CB potential of Fe_2O_3/C composite is 0.24 eV, which is consistent with the result in Fig. 3d [43]. Therefore, the abundant surface C–O and Fe–O groups in the composite are in favor of the adsorption of H_2O_2 and organic pollutants, which could promote the catalytic activity.

3.2. Catalytic performance of Fe_2O_3/C composite

According to the above structure analysis, the Fe_2O_3/C composite should have enhanced catalytic activity compared with Fe_2O_3 and C. A mild test condition (pH = 7, ambient temperature and simulated sunlight) was applied in our experiment. In addition, the catalytic performance of the Fe_2O_3/C composite as heterogeneous Fenton catalyst was studied by degrading Rhodamine B (RhB) and ibuprofen, which

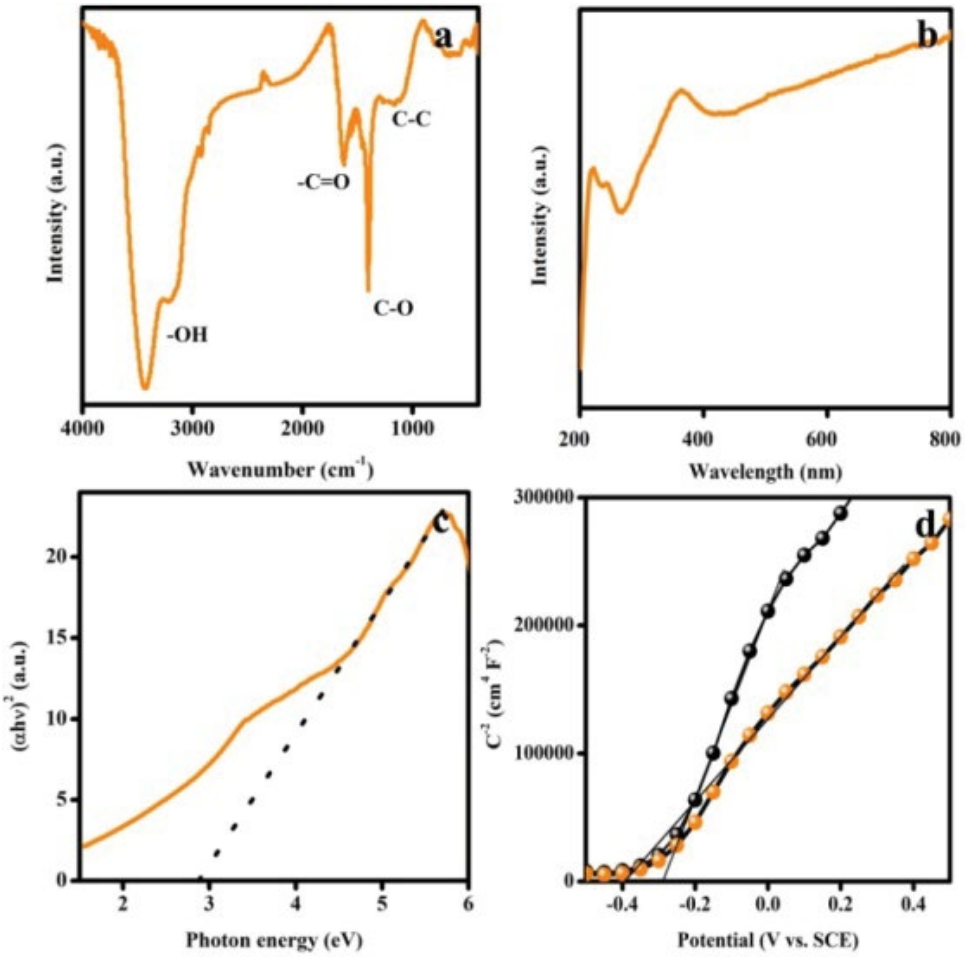

Fig. 3. (a) FTIR spectrum, (b) ultraviolet-visible diffusive reflectance spectra, (c) transformed diffuse reflectance spectra of Fe_2O_3/C composite and (d) Mott–Schottky plots of Fe_2O_3 and Fe_2O_3/C composite.

are dyes and drug pollutants, respectively, in the solution. Therefore, the Fenton catalytic activities of the Fe_2O_3, C and Fe_2O_3/C composite on RhB degradation were first investigated (Fig. 5a), which shows that the Fe_2O_3/C composite has the best Fenton catalytic activity than Fe_2O_3 and C, suggesting the great contribution of the composite structure of Fe_2O_3/C. In Fig. 5b, the plot of $-\ln(C/C_0)$ vs. irradiation time of all the three Fenton catalysts shows that the degradation constant (k) of the Fe_2O_3/C composite (0.014 min^{-1}) is also obviously the best than that of the Fe_2O_3 (0.003 min^{-1}) and C (0.006 min^{-1}; Table S1). However, all the degradation over the Fe_2O_3, C and Fe_2O_3/C composite are incomplete after 30 min. The degradation activity of the Fe_2O_3/C composite is still unsatisfactory. Notably, the Fenton catalytic activity of the Fe_2O_3/C composite was boosted after using BQ as the cocatalyst (Fig. 5c), which indicates that the degradation over the Fe_2O_3/C composite reaches complete after 30 min. The degradation constant (k) of the Fe_2O_3/C composite with BQ addition is 0.142 min^{-1}, which is 10.14 times as many as that without BQ addition (Fig. 5d, Table S2). But the BQ addition has small contribution on the Fenton catalytic activities of the Fe_2O_3 and C (Fig. 5c).

We further studied the content effect of carbon in the Fe_2O_3/C composite on the catalytic activity with BQ addition (Fig. S5a), which indicates that the degradation rates over Fe_2O_3/C composite reach 77% and 86% when the contents of carbon in the composite are 30 wt% and 70 wt%, respectively. It indicates that the carbon effectively increases the Fenton catalytic activity of Fe_2O_3. Since the carbon shows poor Fenton catalytic activity (Fig. 5), the main contribution of carbon in the Fe_2O_3/C composite is to enhance the adsorption of RhB. Furthermore, considering the great contribution of BQ on the enhanced Fenton catalytic activity, we further investigated the effect of BQ content on the catalysis (Fig. S5b), demonstrating that the 3 wt% BQ in the solution is the optimized condition. The Fenton catalytic activity of the Fe_2O_3/C composite under darkness was also studied, which shows that the degradation rate is 70% after 30 min in the presence of BQ, indicating the importance of simulated sunlight in the Fenton catalysis. We further investigated the effect of calcination temperature (300°C, 350°C and 400°C) on the Fenton catalytic activity (Fig. S6a), indicating that the calcination temperature at 350°C is the optimized condition in our experiments. To further verify the synergistic reaction of Fe_2O_3/C composite, we also measured the Fenton catalytic activity of the mixture of Fe_2O_3 and carbon (Fig. S6b), which indicates that the degradation rate of the mixture just reaches 55% in the presence of BQ. Meanwhile, the degradation of

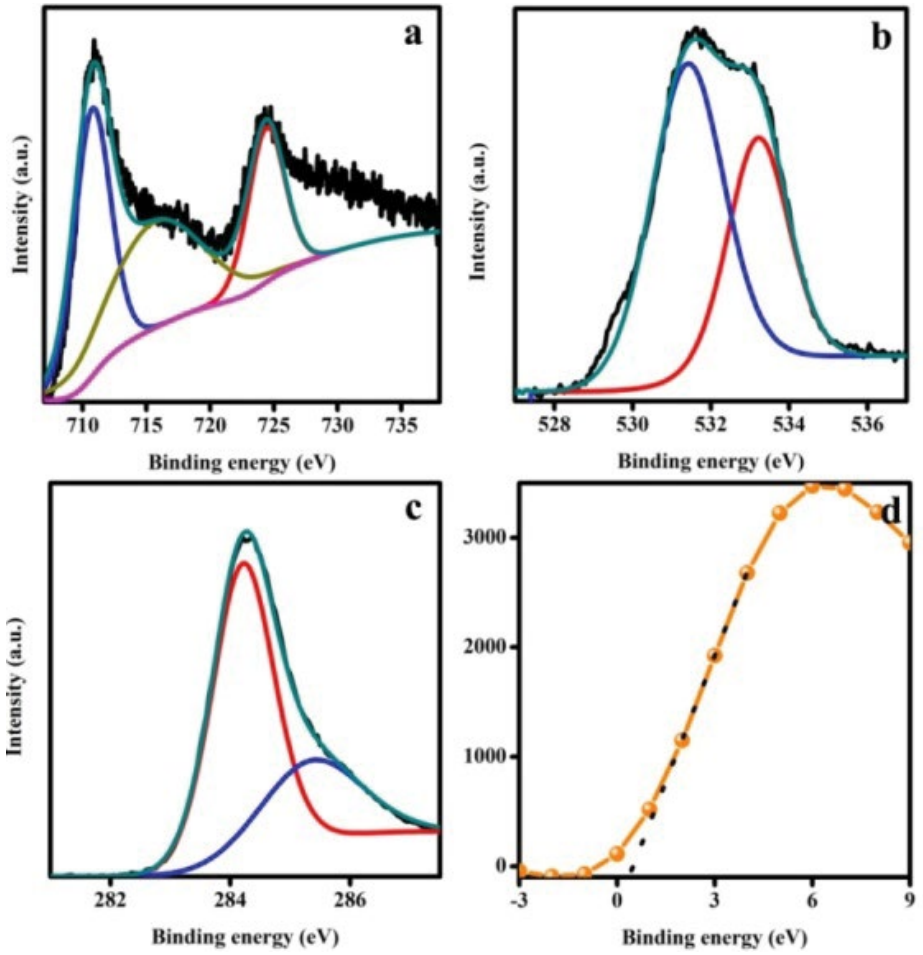

Fig. 4. XPS spectrums of (a) Fe 2p, (b) O1s, (c) C 1s and (d) Fe_2O_3/C composite.

ibuprofen over the Fe_2O_3, C and Fe_2O_3/C composite with BQ as cocatalyst was also measured (Fig. S7), which indicates that the catalytic activity of Fe_2O_3/C composite with BQ is highest than that of Fe_2O_3 and C with BQ. Therefore, the Fe_2O_3, carbon and BQ in the photo-Fenton catalytic system provide a synergistic reaction to enhance the catalytic activity. Moreover, considering that BQ is also a toxicological intermediate [44,45], we also measured the content of BQ after degradation (Figs. S8a and b), which indicates that the BQ was also degraded in the Fenton catalytic process. Therefore, the BQ would not cause secondary pollution to water.

To study the structure stability of the Fe_2O_3/C composite, the Fenton catalytic stability was evaluated by cycling degradation experiment (Fig. S9), which shows that the Fe_2O_3/C composite shows significant stability during the repeated catalytic reactions. The Fe_2O_3/C composite maintains an efficient and stable catalytic activity even after five cycles. Furthermore, we further measured the phase structure and morphology of the Fe_2O_3/C composite after Fenton catalytic (Figs. S10a and b), which indicates that the phase structure and morphology was basically preserved, indicating the super structure stability of the Fe_2O_3/C composite.

It is worthwhile to note that the surface area is a key factor in catalytic degradation, which provides abundant active sites and strengthens the adsorption amount of organic pollutants [46–48]. According to the Fenton catalytic activity measurements in Fig. 5, the Fe_2O_3/C composite obviously adsorbed more RhB molecules than Fe_2O_3 and C. Therefore, we further measured the surface areas of the Fe_2O_3, C and Fe_2O_3/C composite by Brunauer–Emmett–Teller (BET) measurements (Fig. S11). The surface areas of the Fe_2O_3, C and Fe_2O_3/C composite are 5.0, 11.0 and 24 m^2/g, respectively. The composite structure can effectively increase the surface area of Fe_2O_3 and C. The biggest surface area of the Fe_2O_3/C composite than that of Fe_2O_3 and C indicates that the composite has abundant active sites and strong adsorption ability. To further prove this viewpoint, we also measured the adsorption amount of RhB on the Fe_2O_3, C and Fe_2O_3/C composite (Fig. S12). Notably, the adsorption amount on the Fe_2O_3/C composite is the biggest, which is 12.3 times and 2.1 times as many as that on Fe_2O_3 and C, respectively.

The charge separation plays an important role on the photo-Fenton catalytic process. Therefore, we further measured the photocurrents response of the Fe_2O_3, C and Fe_2O_3/C composite (Fig. 6a), which demonstrate that the photocurrent was increased sharply when the light was on, but dropped to minimum in darkness. Although all the three samples displayed steady and reproducible on-off cycles, the photocurrent density of the Fe_2O_3/C composite is the highest,

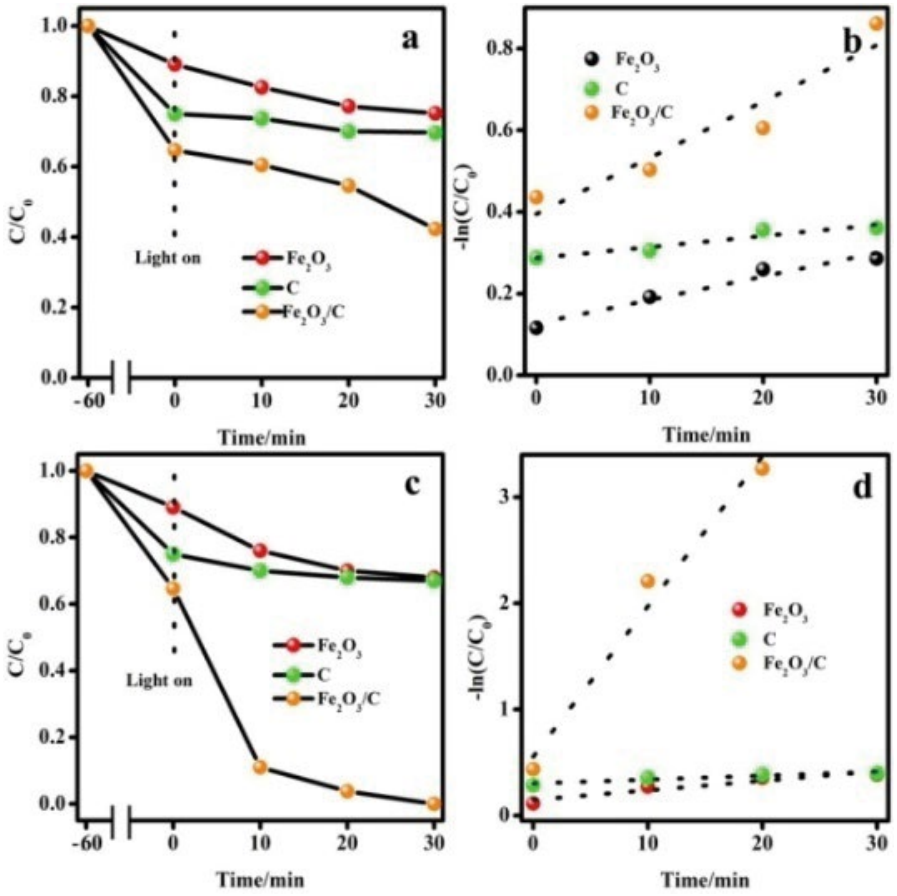

Fig. 5. Photo-Fenton catalytic activity of the Fe_2O_3, C and Fe_2O_3/C composite (a) without BQ and (c) with BQ on RhB degradation, the kinetic plots for the Fe_2O_3, C and Fe_2O_3/C composite (b) without BQ and (d) with BQ.

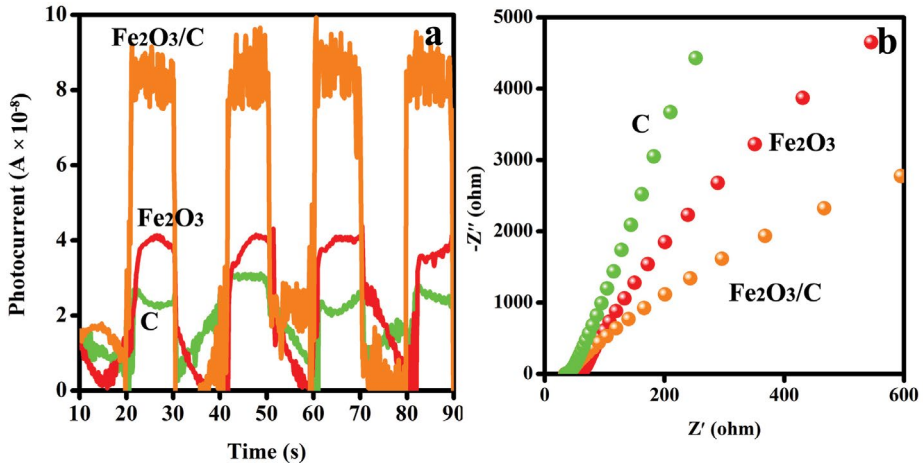

Fig. 6. (a) photocurrents response and (b) electrochemical impedance spectra (Nyquist plot) of the Fe_2O_3, C and Fe_2O_3/C composite.

suggesting the highest separation efficiency of charge carries of the Fe_2O_3/C composite [49–52]. Moreover, the EIS has also been carried out to study the charge transfer process on the interfacial contact [53–55]. As shown in Fig. 6b, the arc radius of the Fe_2O_3/C composite is the smallest than those of Fe_2O_3 and C, indicating that the Fe_2O_3/C composite has the fastest interfacial charge transfer and the highest separation efficiency of photo-generated charge carriers among them. The results suggest that the composite structure between Fe_2O_3 and C is beneficial for the enhancement of photo-Fenton catalytic activity.

The •OH radicals produced by the decomposition of hydrogen peroxide have strong oxidation capacities to degrade organic pollutant, which play a central role in

Fenton catalysis. Therefore, the scavenger (isopropyl alcohol, IPA) used as probe was introduced into the Fenton catalysis to detect the •OH radicals in the RhB degradation system (Fig. 7a). As shown in Fig. 7a, the degradation rate is suppressed to 44% from 58% over the Fe_2O_3/C composite without BQ addition, indicating that the oxidation process proceeds through direct attack of •OH radical to organic compounds. In contrast, the degradation rate is obviously suppressed to 61% with BQ addition. The suppressed degradation degree over Fe_2O_3/C with BQ (39%) is bigger than that without BQ (24%). According to the literatures, the suppressed degradation degree can reflect the production of active species [56]. Therefore, the production of •OH radicals over the Fe_2O_3/C composite greatly increased by the introduction of BQ. To further prove this viewpoint, the H_2O_2 conversion to •OH radicals was also measured (Fig. S13a), which indicates that the production of •OH radicals over Fe_2O_3/C composite with BQ is bigger than that without BQ, suggesting the great contribution of BQ on the conversion of H_2O_2 to •OH radicals. The BQ is the trapping agent of $•O_2H$ radicals, which can effectively promote the consumption of $•O_2H$ radicals and further increase the production of Fe^{II}. The increased content of Fe^{II} on the composite surface can react with H_2O_2 to produce •OH radicals. Furthermore, since the BQ has strong oxidizability, the photogenerated electrons in the Fe_2O_3/C composite maybe captured by the BQ to promote the separation of photogenerated electron–hole pairs. Therefore, we further detected the holes in the photocatalytic systems of the Fe_2O_3/C composite under solar light by adding ammonium oxalate (AO) as molecular probe (Fig. S13b), which indicates that the degradation rate over Fe_2O_3/C composite as photocatalyst decreased to 25% from 32% after adding BQ, suggesting that the production of holes in the photocatalysis increased by the introduction of BQ. We further measured the catalytic degradation rate over Fe_2O_3/C composite as photo-Fenton catalyst in the presence of ammonium oxalate (Fig. 7b), which indicates that the degradation rate decreased after adding AO as molecular probe. These results imply that the separation efficiency of photogenerated electron hole pairs in Fe_2O_3/C composite increased due to the capture of electrons by BQ.

Based on experimental results, the enhanced photo-Fenton catalytic performance of the Fe_2O_3/C composite with BQ addition may be caused by a synergy mechanism (Fig. 8). The heterogeneous Fenton reaction (Fe^{III}-H_2O_2) relies on the catalytic conversion of H_2O_2 to •OH radicals. Unfortunately, the rate-determining step of the reaction ($Fe^{III} + H_2O_2 \rightarrow Fe^{II} + O_2^-$) greatly limits the catalytic activity. The BQ can trap the $•O_2^-$ radical to promote the production of Fe^{II}, which could further react with H_2O_2 to generate •OH radicals. According to Fig. 8, the contribution of BQ on the enhanced photo-Fenton catalytic activity over the Fe_2O_3/C composite is the biggest than that over Fe_2O_3 and C, indicating the synergistic interaction of surface adsorption and radical-scavenging caused by BQ. Although the carbon has better surface adsorption ability for BQ than Fe_2O_3, the carbon is unable to decompose hydrogen peroxide to produce •OH radicals. Conversely, the Fe_2O_3 can react with H_2O_2 to produce $•O_2^-$ radicals, but the weak surface adsorption for BQ on Fe_2O_3 limits the radical scavenging. Therefore, the addition of BQ has no significant effect on Fenton catalytic activities of Fe_2O_3 and C. Because the reactions of H_2O_2 decompose and RhB degradation mainly occur on the Fe_2O_3/C composite surface, the adsorption of BQ on the Fe_2O_3/C composite surface is vitally important. As for Fe_2O_3/C composite, the

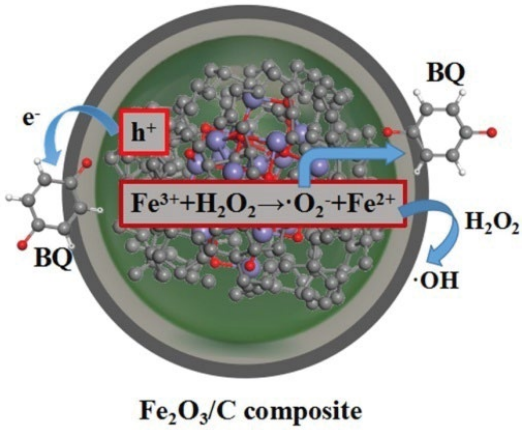

Fig. 8. Schematic illustration of the mechanism for the enhanced photo-Fenton catalytic performance of Fe_2O_3/C composite with BQ addition.

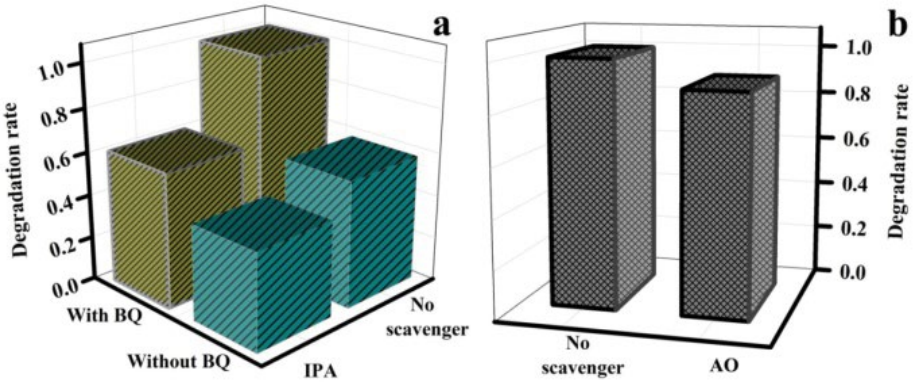

Fig. 7. (a) Trapping experiment of •OH radicals and (b) catalytic degradation rate in an aqueous solution saturated with air and oxygen over Fe_2O_3/C composite.

high surface area of the composite caused by carbon greatly increase the surface adsorption for BQ, which promotes the $^{\bullet}O_2^-$radical scavenging, and further promote the production of Fe^{II}. Furthermore, the Fe_2O_3/C composite can also produce photogenerated electron hole pair in the photo-Fenton catalysis process. The BQ can also react with the photogenerated electron to promote the separation efficiency (Fig. S13b). Furthermore, the BQ can also be degraded due to the excess $^{\bullet}OH$ radicals produced in the Fenton process. The holes with strong oxidation can degrade organic pollutant to further improve the photo-Fenton catalytic activity.

4. Conclusion

In this work, a novel Fenton catalytic system of Fe_2O_3/C-(1,4-benzoquinone) has been successfully developed, which shows greatly enhanced Fenton catalytic activities for RhB degradation than Fe_2O_3/C. The carbon in the Fe_2O_3/C composite effectively promotes the surface adsorption of RhB and BQ. The Fe_2O_3 acts as main Fenton catalyst in the catalysis process. The BQ acts as a trapping agent of $^{\bullet}O_2^-$ radical and photogenerated electrons in the photo-Fenton catalysis. The existence of BQ in the system promotes the production of Fe^{II} and photogenerated hole, resulting in enhanced degradation activity. The Fe_2O_3/C-(1,4-benzoquinone) system could shed new light on the novel Fenton catalysis in the applications of environmental pollution and energy crisis.

Acknowledgments

This work is supported by the key research and development plan of Jining City, and the key research and development plan of Shandong Province (2019GSF110007, 2019GNC106039).

References

[1] X. Duan, H. Sun, S. Wang, Metal-free carbocatalysis in advanced oxidation reactions, Accounts Chem. Res., 51 (2018) 678–687.
[2] P. Shao, J. Tian, F. Yang, X. Duan, S. Gao, W. Shi, X. Luo, F. Cui, S. Luo, S. Wang, Identification and regulation of active sites on nanodiamonds: establishing a highly efficient catalytic system for oxidation of organic contaminants, Adv. Funct. Mater., 28 (2018) 1705295.
[3] F.C. Moreira, R.A.R. Boaventura, E. Brillas, V.J.P. Vilar, Electrochemical advanced oxidation processes: a review on their application to synthetic and real wastewaters, Appl. Catal., B, 202 (2017) 217–261.
[4] S. Wang, H. Yang, Z. Yi, X. Wang. Enhanced photocatalytic performance by hybridization of Bi_2WO_6 nanoparticles with honeycomb-like porous carbon skeleton, J. Environ. Manage., 248 (2019) 109341.
[5] X. Zhao, H. Yang, Z. Cui, Z. Yi, H. Yu, Synergistically enhanced photocatalytic performance of $Bi_4Ti_3O_{12}$ nanosheets by Au and Ag nanoparticles, J. Mater. Sci.-Mater. Electron., 30 (2019) 13785–13796.
[6] T. Guo, K. Wang, G. Zhang, X. Wu, A novel α-Fe_2O_3@g-C_3N_4 catalyst: Synthesis derived from Fe-based MOF and its superior photo-Fenton performance, Appl. Surf. Sci., 469 (2019) 331–339.
[7] X. Nguyen, G. Zhang, O. Yang, Mesocrystalline Zn-Doped Fe_3O_4 Hollow submicrospheres: formation mechanism and enhanced photo-Fenton catalytic performance, ACS Appl. Mater. Interfaces, 9 (2017) 8900–8909.
[8] C. Xiao, J. Li, G. Zhang, Synthesis of stable burger-like α-Fe_2O_3 catalysts: Formation mechanism and excellent photo-Fenton catalytic performance, J. Clean. Prod., 180 (2018) 550–559.
[9] S. Guo, G. Zhang, J. Yu, Enhanced photo-Fenton degradation of rhodamine B using graphene oxide–amorphous $FePO_4$ as effective and stable heterogeneous catalyst, J. Colloid Interface Sci., 448 (2015) 460–466.
[10] M. Cheng, C. Lai, Y. Liu, G. Zeng, D. Huang, C. Zhang, L. Qin, L. Hu, C. Zhou, W. Xiong, Metal-organic frameworks for highly efficient heterogeneous Fenton-like catalysis, Coord. Chem. Rev., 368 (2018) 80–92.
[11] S.O. Ganiyu, M. Zhou, C.A.M. Huitle, Heterogeneous electro-Fenton and photoelectro-Fenton processes: a critical review of fundamental principles and application for water/wastewater treatment, Appl. Catal. B, 235 (2018) 103–129.
[12] V.P. Nogueiras, E. Rosales, M. Pazos, M.Á. Sanromán, Current advances and trends in electro-Fenton process using heterogeneous catalysts - a review, Chemosphere, 201 (2018) 399–416.
[13] H. Dai, S. Xu, J. Chen, X. Miao, J. Zhu, Oxalate enhanced degradation of Orange II in heterogeneous UV-Fenton system catalyzed by Fe_3O_4@γ-Fe_2O_3 composite, Chemosphere, 199 (2018) 147–153.
[14] R. Edla, A. Tonezzer, M. Orlandi, N. Patel, R. Fernandes, N. Bazzanella, K. Date, D.C. Kothari, A. Miotello, 3D hierarchical nanostructures of iron oxides coatings prepared by pulsed laser deposition for photocatalytic water purification, Appl. Catal. B, 219 (2017) 401–411.
[15] L. Wan, H. Song, J. Ma, Y. Ren, X. Cheng, J. Su, Q. Yue, Y. Deng, Polymerization-induced colloid assembly route to iron oxide-based mesoporous microspheres for gas sensing and Fenton catalysis, ACS Appl. Mater. Interface, 10 (2018) 13028–13039.
[16] S. Giannakis, S. Liu, A. Carratalà, S. Rtimi, M.T. Amiri, M. Bensimon, C. Pulgarin, Iron oxide-mediated semiconductor photocatalysis vs. heterogeneous photo-Fenton treatment of viruses in wastewater. impact of the oxide particle size, J. Hazard. Mater., 339 (2017) 223–231.
[17] Z. Wu, W. Zhu, M. Zhang, Y. Lin, N. Xu, F. Chen, D. Wang, Z. Chen, Adsorption and synergetic Fenton-like degradation of methylene blue by a novel mesoporous α-Fe_2O_3/SiO_2 at neutral pH, Ind. Eng. Chem. Res., 57 (2018) 5539–5549.
[18] S.H. Yoo, D. Jang, H.-I. Joh, S. Lee, Iron oxide/porous carbon as a heterogeneous Fenton catalyst for fast decomposition of hydrogen peroxide and efficient removal of methylene blue, J. Mater. Chem. A, 5 (2017) 748–755.
[19] L. Zhou, L. Wang, J. Zhang, J. Lei, Y. Liu, Well-dispersed Fe_2O_3 nanoparticles on g-C_3N_4 for efficient and stable photo-Fenton photocatalysis under visible-light irradiation, Eur. J. Inorg. Chem., 34 (2016) 5387–5392.
[20] J.C. Espinosa, C. Catalá, S. Navalón, B. Ferrer, M. Álvaro, H. García, Iron oxide nanoparticles supported on diamond nanoparticles as efficient and stable catalyst for the visible light assisted Fenton reaction, Appl. Catal. B, 226 (2018) 242–251
[21] Y. Liu, W. Jin, Y. Zhao, G. Zhang, W. Zhang, Enhanced catalytic degradation of methylene blue by α-Fe_2O_3/graphene oxide via heterogeneous photo-Fenton reactions, Appl. Catal. B, 206 (2017) 642–652.
[22] Z. Xu, C. Huang, L. Wang, X. Pan, L. Qin, X. Guo, G. Zhang, Sulfate functionalized Fe_2O_3 nanoparticles on TiO_2 nanotube as efficient visible light-active photo-Fenton catalyst, Ind. Eng. Chem. Res., 54 (2015) 4593–4602.
[23] J. Ma, W. Ma, W. Song, C. Chen, Y. Tang, J. Zhao, Fenton degradation of organic pollutants in the presence of low-molecular-weight organic acids: cooperative effect of quinone and visible light, Environ. Sci. Technol., 40 (2006) 618–624.
[24] W. Zhou, J. Gao, Ha. Zhao, X Meng, S. Wu, The role of quinone cycle in Fe^{2+}–H_2O_2 system in the regeneration of Fe^{2+}, Environ. Technol., 38 (2017) 1887–1896.
[25] J.S. Cho, Y.J. Hong, Y.C. Kang, Design and synthesis of bubble-nanorod-structured Fe_2O_3 -carbon nanofibers as advanced anode material for Li-ion batteries, ACS Nano, 9 (2015) 4026–4035.
[26] F. Han, D. Li, W.-C. Li, C. Lei, Q. Sun, A.-H. Lu, Nanoengineered polypyrrole-coated Fe_2O_3@C multifunctional composites with an improved cycle stability as lithium-ion anodes, Adv. Funct. Mater., 23 (2013) 1692–1700.

[27] N. Zhang, X. Han, Y. Liu, X. Hu, Q. Zhao, J. Chen, 3D Porous γ-Fe_2O_3@C nanocomposite as high-performance anode material of Na-ion batteries, Adv. Energy Mater., 5 (2015) 1401123.
[28] B.H. Hameed, A.T.M. Din, A.L. Ahmad, Adsorption of methylene blue onto bamboo-based activated carbon: Kinetics and equilibrium studies, J. Hazard. Mater., 141 (2007), 819–825.
[29] K.C. Bedin, A.C. Martins, A.L. Cazetta, O. Pezoti, V.C. Almeida, KOH-activated carbon prepared from sucrose spherical carbon: Adsorption equilibrium, kinetic and thermodynamic studies for Methylene Blue removal, Chem. Eng. J., 286 (2016) 476–484.
[30] J. Jiang, X. Zhang, X. Zhu, Y. Li, Removal of intermediate aromatic halogenated DBPs by activated carbon adsorption: a new approach to controlling halogenated DBPs in chlorinated drinking water, Environ. Sci. Technol., 51 (2017) 3435–3444.
[31] F. Xu, Z. Tang, S. Huang, L. Chen, Y. Liang, W. Mai, H. Zhong, R. Fu, D. Wu, Facile synthesis of ultrahigh-surface-area hollow carbon nanospheres for enhanced adsorption and energy storage, Nat. Commun., 6 (2015) 7221.
[32] J. Zhang, S. Wu, W. Bi, X. Zhao, G. Liu, Z-scheme Fe_2O_3-doped Cu_2O as an efficient photo-Fenton-like catalyst for degradation of phenol, Mater. Lett., 234 (2019) 13–16.
[33] G. Liu, X. Zhao, J. Zhang, S. Liu, J. Sha, Z-scheme Ag_3PO_4/POM/GO heterojunction with enhanced photocatalytic performance for degradation and water splitting, Dalton Trans., 47 (2018) 6225–6232.
[34] J. Zhang, X. Zhao, M. Zhong, M. Yang, Y. Lian, G. Liu, S. Liu, An iron oxychloride/reduced graphene oxide heterojunction with enhanced catalytic performance as a photo-Fenton catalyst, Eur. J. Inorg. Chem., 26 (2018) 3080–3087.
[35] J. Zhang, G. Liu, S. Liu, 2D/2D FeOCl/graphite oxide heterojunction with enhanced catalytic performance as a photo-Fenton catalyst, New J. Chem., 42 (2018) 6896–6902.
[36] T. Yamashita, P. Hayes, Analysis of XPS spectra of Fe^{2+} and Fe^{3+} ions in oxide materials, Appl. Surf. Sci., 254 (2008) 2441–2449.
[37] H. Cui, Y. Liu, W. Ren, Structure switch between α-Fe_2O_3, γ-Fe_2O_3 and Fe_3O_4 during the large scale and low temperature sol-gel synthesis of nearly monodispersed iron oxide nanoparticles, Adv. Powder Technol., 24 (2013) 93–97.
[38] H.A. Alalwan, S.E. Mason, V.H. Grassian, D.M. Cwiertny, α-Fe_2O_3 nanoparticles as oxygen carriers for chemical looping combustion: an integrated materials characterization approach to understanding oxygen carrier performance, reduction mechanism, and particle size effects, Energy Fuels, 32 (2018) 7959–7970.
[39] Z. Li, S. Ganapathy, Y. Xu, Q. Zhu, W. Chen, I. Kochetkov, C. George, L.F. Nazar, M. Wagemaker, Fe_2O_3 nanoparticle seed catalysts enhance cyclability on deep (dis)charge in aprotic Li-O_2 batteries, Adv. Energy Mater., 8 (2018) 1703513.
[40] X. Zhao, X. Yi, S. Tian, J. Zhang, Excellent photocatalytic degradation and disinfection performance of a novel bifunctional Ag@AgSCN nanostructure with exposed {-112} facets, New J. Chem., 42 (2018) 11811–11818.
[41] Y. Li, W. Ho, K. Lv, B. Zhu, S.C. Lee, Carbon vacancy-induced enhancement of the visible light-driven photocatalytic oxidation of NO over g-C_3N_4 nanosheets, Appl. Surf. Sci., 430 (2018) 380–389.
[42] X. Zhao, H. Yang, H. Zhang, Z. Cui, W. Feng. Surface-disorder-engineering-induced enhancement in the photocatalytic activity of $Bi_4T_{i3}O_{12}$ nanosheets, Desal. Wat. Treat., 145 (2019) 326–336.
[43] J.L. Bolton, M.A. Trush, T.r M. Penning, G. Dryhurst, T.J. Monks, Role of quinones in toxicology, Chem. Res. Toxicol., 13 (2000) 135–160.
[44] J. Wang, Z. Bai, Fe-based catalysts for heterogeneous catalytic ozonation of emerging contaminants in water and wastewater, Chem. Eng. J., 312 (2017) 79–98.
[45] Y. Liu, X. Liu, Y. Zhao, D.D. Dionysiou, Aligned α-FeOOH nanorods anchored on a graphene oxide-carbon nanotubes aerogel can serve as an effective Fenton-like oxidation catalyst, Appl. Catal., B, 213 (2017) 74–86.
[46] J. Piella, F. Merkoçi, A. Genç, J. Arbiol, N.G. Bastús, V. Puntes, Probing the surface reactivity of nanocrystals by the catalytic degradation of organic dyes: the effect of size, surface chemistry and composition, J. Mater. Chem. A, 5 (2017) 11917–11929.
[47] D.K.L. Chan, J.C. Yu, Facile synthesis of carbon- and oxygen-rich graphitic carbon nitride with enhanced visible-light photocatalytic activity, Catal. Today, 310 (2018) 26–31.
[48] N.L. De Silva, A.C.A. Jayasundera, A. Folger, O. Kasian, S. Zhang, C.-F. Yan, C. Scheu, J. Bandara, Superior solar-to-hydrogen energy conversion efficiency by visible light-driven hydrogen production via highly reduced Ti^{2+}/Ti^{3+} states in a blue titanium dioxide photocatalyst, Catal. Sci. Technol., 8 (2018) 4657–4664.
[49] H. Li, Y. Sun, Z.-Y. Yuan, Y.-P. Zhu, T.-Y. Ma, Titanium phosphonate based metal-organic frameworks with hierarchical porosity for enhanced photocatalytic hydrogen evolution, Angew. Chem. Int. Edit., 57 (2018) 3222–3227.
[50] S.L. Wang, Y. Zhu, X. Luo, Y. Huang, J. Chai, T.I. Wong, G.Q. Xu, 2D WC/WO_3 Heterogeneous hybrid for photocatalytic decomposition of organic compounds with Vis–NIR light, Adv. Funct. Mater., 28 (2018) 1705357–1705365.
[51] T. Xu, L. Zhang, H. Cheng, Y. Zhu, Significantly enhanced photocatalytic performance of ZnO via graphene hybridization and the mechanism study, Appl. Catal., B, 101 (2011) 382–387.
[52] L.-W. Zhang, H.-B. Fu, Y.-F. Zhu, Efficient TiO_2 photocatalysts from surface hybridization of TiO_2 particles with graphite-like carbon, Adv. Funct. Mater., 18 (2008) 2180–2189.
[53] J. Zhang, X. Chen , K. Takanabe, K. Maeda, K. Domen, J.D. Epping, X. Fu, M. Antonietti, X. Wang, Synthesis of a carbon nitride structure for visible-light catalysis by copolymerization, Angew. Chem. Int. Edit., 49 (2010) 441–444.
[54] J. Shi, Z. Ai, L. Zhang, Fe@Fe_2O_3 core-shell nanowires enhanced Fenton oxidation by accelerating the Fe(III)/Fe(II) cycles, Water Res., 59 (2014) 145–153.
[55] H. Niu, Y. Zheng, S. Wang, L. Zhao, S. Yang, Y. Cai, Continuous generation of hydroxyl radicals for highly efficient elimination of chlorophenols and phenols catalyzed by heterogeneous Fenton-like catalysts yolk/shell Pd@Fe_3O_4@metal organic frameworks, J. Hazard. Mater., 346 (2018) 174–183.
[56] J. Yu, Q. Xiang, M. Zhou, Preparation, characterization and visible-light-driven photocatalytic activity of Fe-doped titania nanorods and first-principles study for electronic structures, Appl. Catal., B, 90 (2009) 595–602.

Supporting information:

Boosting photo-Fenton catalytic performance of Fe_2O_3/C composite with 1,4-benzoquinone as cocatalyst

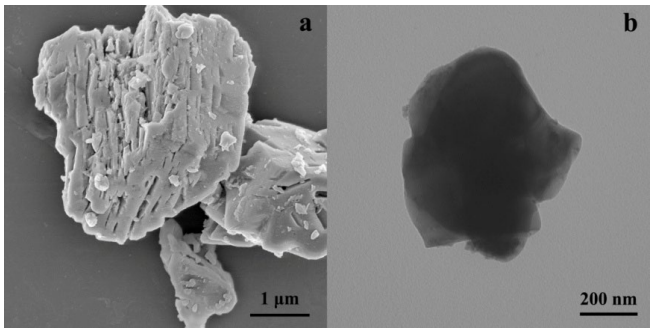

Fig. S1. (a) SEM image and (b) TEM image of Fe_2O_3.

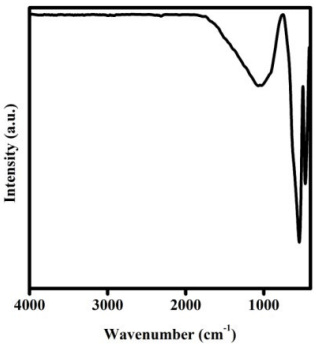

Fig. S2. FTIR spectra of Fe_2O_3.

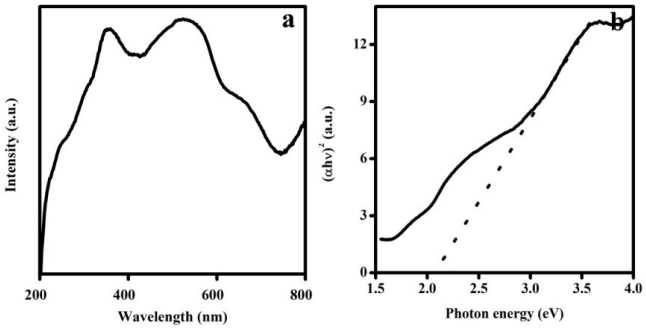

Fig. S3. (a) Ultraviolet-visible diffusive reflectance spectra and (b) transformed diffuse reflectance spectra of Fe_2O_3.

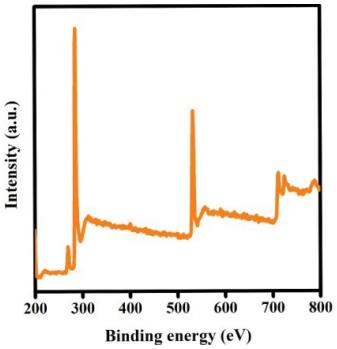

Fig. S4. Full-range XPS spectrum of Fe_2O_3/C composite.

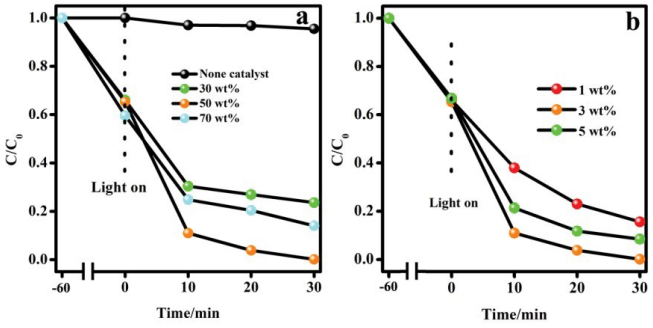

Fig. S5. Photo-Fenton catalytic activity of Fe_2O_3/C composite with (a) different carbon content and (b) BQ content.

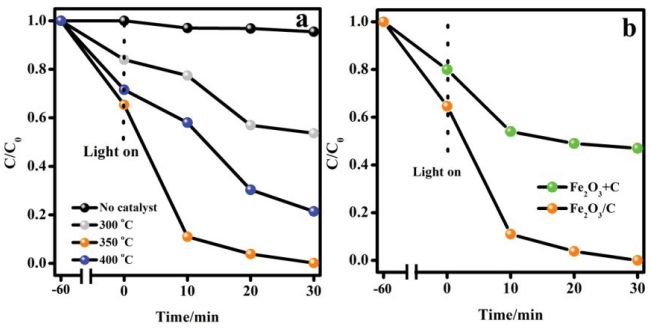

Fig. S6. Photo-Fenton catalytic activity of Fe_2O_3/C composite with (a) different calcination temperature and (b) of the mixture of Fe_2O_3 and carbon.

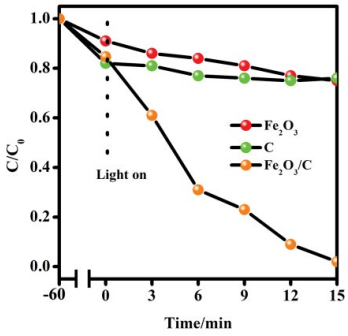

Fig. S7. Photo-Fenton catalytic activity of the Fe_2O_3, C and Fe_2O_3/C composite with BQ on ibuprofen degradation.

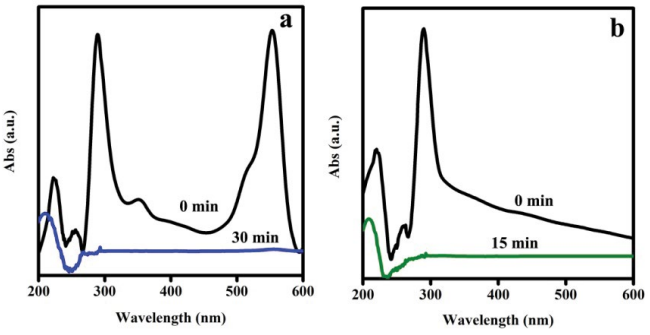

Fig. S8. Photocatalytic degradation curves of (a) RhB and (b) ibuprofen over Fe_2O_3/C composite with BQ addition.

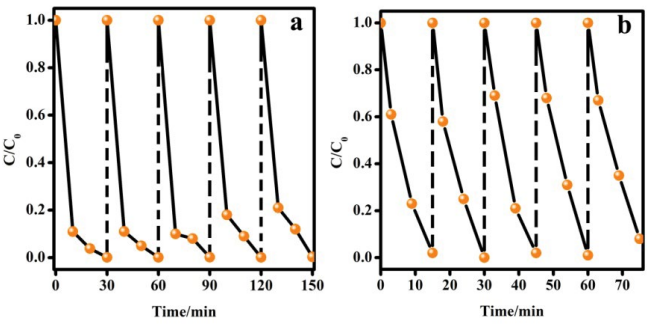

Fig. S9. Cycling degradation of (a) RhB and (b) ibuprofen over Fe_2O_3/C composite with BQ addition.

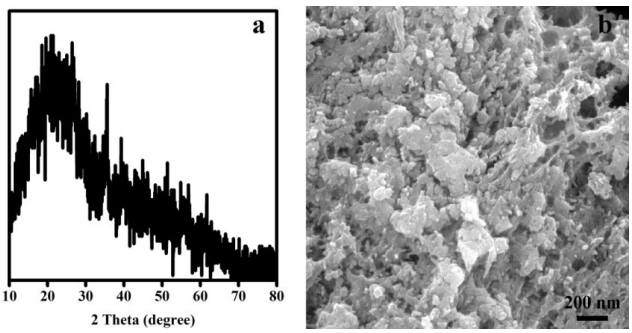

Fig. S10. (a) XRD pattern and (b) SEM image of Fe_2O_3/C composite after reaction.

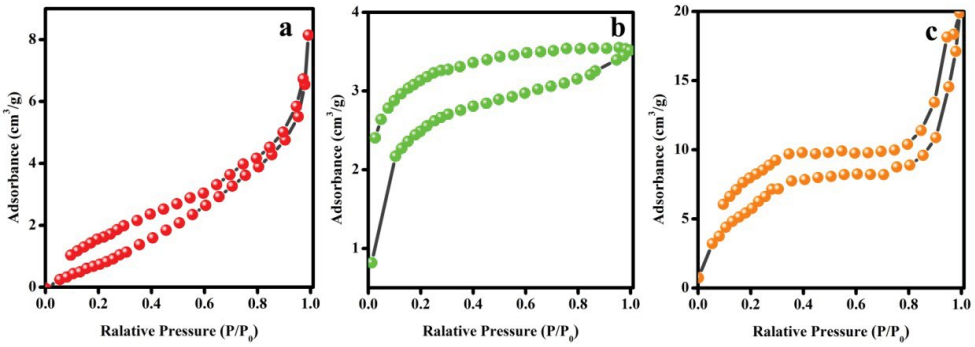

Fig. S11. N_2 adsorption–desorption isotherms of Fe_2O_3, C and Fe_2O_3/C composite.

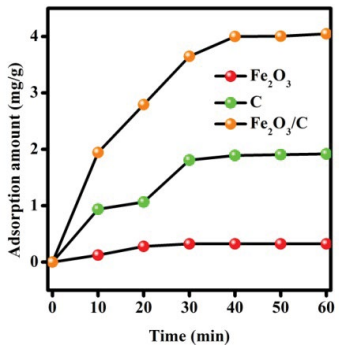

Fig. S12. Adsorption amount of RhB on Fe_2O_3, C and Fe_2O_3/C composite.

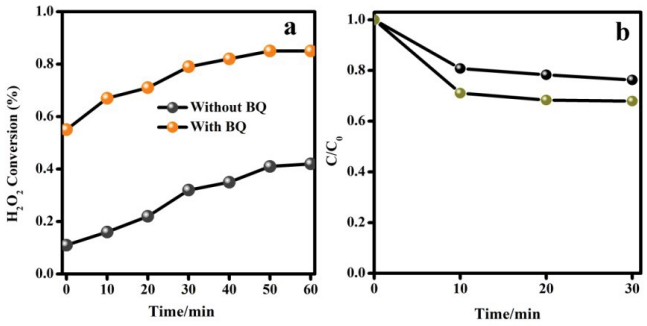

Fig. S13. (a) H_2O_2 conversion over Fe_2O_3/C composite with BQ and without BQ, (b) trapping experiment of h^+ over Fe_2O_3/C composite with BQ.

Table S1
Rate constants (k) of Fenton catalytic degradation of RhB over the Fe_2O_3, C and Fe_2O_3/C composite without BQ

Catalyst	k (min^{-1})
Fe_2O_3	0.003
C	0.006
Fe_2O_3/C	0.014

Table S2
Rate constants (k) of Fenton catalytic degradation of RhB over the Fe_2O_3, C and Fe_2O_3/C composite with BQ

Catalyst	k (min^{-1})
Fe_2O_3	0.004
C	0.009
Fe_2O_3/C	0.142